ELSEVIER

Earth and Planetary Science Letters 136 (1995) 495–510

EPSL

Extending the astronomical (polarity) time scale into the Miocene

F.J. Hilgen [a], W. Krijgsman [b], C.G. Langereis [b], L.J. Lourens [a], A. Santarelli [c], W.J. Zachariasse [a]

[a] *Department of Geology, Institute of Earth Sciences, Budapestlaan 4, 3584 CD Utrecht, The Netherlands*
[b] *Paleomagnetic Laboratory "Fort Hoofddijk", Budapestlaan 17, 3584 CD Utrecht, The Netherlands*
[c] *Laboratory of Paleobotany and Palynology, Heidelberglaan 2, 3582 CS Utrecht, The Netherlands*

Received 5 May 1995; accepted 26 October 1995

Abstract

An astronomical time scale is presented for the late Miocene based on the correlation of characteristic sedimentary cycle patterns in marine sections in the Mediterranean to the 65°N summer insolation curve of La90 [1,2] with present-day values for the dynamical ellipticity of the Earth and tidal dissipation by the moon. This correlation yields ages for all sedimentary cycles and hence also for the recorded polarity reversals, and planktonic foraminiferal and dinoflagellate events. The Tortonian/Messinian (T/M) boundary placed at the first regular occurrence of the *Globorotalia conomiozea* group in the Mediterranean is dated at 7.24 Ma. The duration of the Messinian is estimated at 1.91 Myr because the Miocene/Pliocene boundary has been dated previously at 5.33 Ma [3]. The new time scale is confirmed by $^{40}Ar/^{39}Ar$ ages of volcanic beds and by the number of sedimentary cycles in the younger part of the Mediterranean Messinian.

.... to correlate these with an astronomical cycle of known period, and to deduce from this correlation an estimate in years of a portion of...

(from: G.K. Gilbert, 1895, Sedimentary measurement of Cretaceous time, *Journal of Geology*, 3, p. 121).

1. Introduction

A recently developed method to construct geological time scales involves the calibration of sedimentary cycles, or other cyclic variations in geological records, to computed time series of the quasi-periodic variations of the Earth's orbit. Following early tuning attempts for the late Pleistocene during the 1960's and early 1970's [4–6], the astronomical time scale is now well established for the last 6 million years [7–11]. This time scale deviates considerably from earlier time scales based on K/Ar dating, and has subsequently been confirmed by radioisotopic ages using the $^{40}Ar/^{39}Ar$ (single crystal) laser fusion dating technique. The new time scale has been successfully applied in paleoclimatic studies [12] and in studies of seafloor spreading history [13]. In addition, the age of fluence monitor standards in radioisotopic (Ar/Ar) dating has been calibrated independently of absolute isotopic abundance measurements by comparison of astronomical and $^{40}Ar/^{39}Ar$ ages for seven polarity reversals over the last 3.5 Myr [14].

In this study, we aim at extending the astronomi-

SSDI 0012-821X(95)00207-3

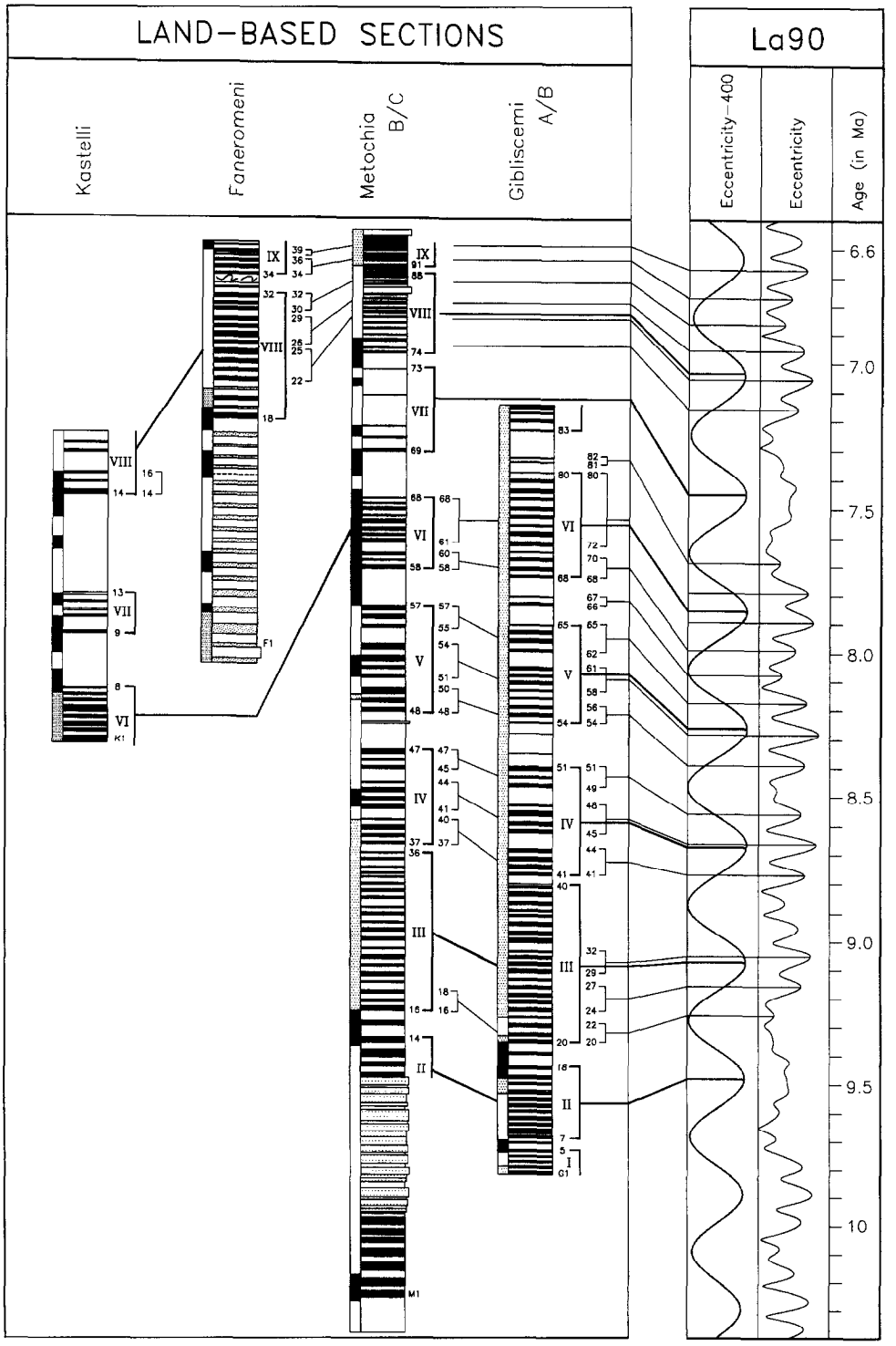
LAND–BASED SECTIONS
Kastelli
Faneromeni
Metochia B/C
Gibliscemi A/B
La90
Eccentricity–400
Eccentricity
Age (in Ma)
6.6
7.0
7.5
8.0
8.5
9.0
9.5
10
IX
VIII
VII
VI
V
IV
III
II
I
F1
M1
K1
G1

cal time scale back in time, into the Miocene. Earlier, Shackleton et al. [8] carried out a preliminary and partial astronomical tuning of GRAPE (Gamma Ray Attenuation Porosity Evaluation) records of ODP Leg 138 sites for the interval between 6 and 10 Ma, while Krijgsman et al. [15] calculated an astronomical duration for a late Miocene polarity sequence on Crete by multiplying the number of sedimentary cycles with the average 21.7 kyr period of precession. The duration of the latter sequence is approximately 10% shorter than that of the correlative part in the geomagnetic polarity time scale (GPTS) of Cande and Kent [16]. Here, we calibrate the sedimentary cycles of the sections from Crete [15] and of older sections from Gavdos and Sicily [17] directly to astronomical target curves. This calibration provides astronomical ages for all sedimentary cycles and hence for the polarity reversals and biostratigraphic datum planes recorded in these Mediterranean sections.

The resulting time scale is then compared with recent polarity time scales of Cande and Kent ([18], CK95) and Shackleton et al. ([8], SCHPS95), with radiometric ($^{40}Ar/^{39}Ar$) ages of volcanic beds, and with the number of sedimentary cycles in the younger, partly evaporitic, part of the Mediterranean Messinian.

2. Cyclostratigraphy of the sections

We have used four Mediterranean sections for the construction of our time scale, namely the Metochia section on Gavdos, the Gibliscemi section on Sicily and the Faneromeni and Kastelli sections on Crete (see fig. 1 in [17] for exact location). The magnetostratigraphy and biostratigraphy of the sections, and the correlation of the magnetostratigraphy to the GPTS of Cande and Kent ([18], CK95) have been discussed in detail by Krijgsman et al. ([17], see also their fig. 7); they showed that the succession starts above chron C5n and continues into chron C3An, and ranges from 9.7 to 6.5 Ma according to CK95. The cyclostratigraphic details and the correlation of the sedimentary cycle patterns to the astronomical solutions are presented in the present paper.

All sections consist of open marine sediments that show cyclic alternations of either whitish-coloured carbonate-rich and grey-coloured carbonate-poor marls (Faneromeni, lower part), or of homogeneous marls and brownish-coloured beds termed sapropels. Sapropels (and the related grey beds) have been labeled in stratigraphical order per section. Their characteristic pattern allows the sections to be correlated in detail. These cyclostratigraphic ("bed-to-bed") correlations are confirmed by the magnetostratigraphy and biostratigraphy (see also fig. 7 in [17]). They reveal minor differences in the number and expression of the cycles, for instance the Gibliscemi section contains additional (thin) sapropels in intervals which correspond to thick homogeneous marly intervals on Gavdos (Fig. 1).

Sapropels in particular display characteristic cycle patterns. A prominent feature is the occurrence of sapropels in both small-scale clusters and large-scale clusters (Fig. 1). Small-scale clusters typically contain 3 or 4 sapropels and are separated from adjacent (small-scale) clusters by a thin, poorly developed sapropel and/or a homogeneous marl bed which is thicker - approximately two times - than a regular homogeneous marl bed. Large-scale clusters typically contain 3 or 4 small-scale clusters and are separated from adjacent clusters by thick homogeneous intervals which only occasionally contain additional thin sapropels. Large-scale clusters are given a roman numerical (see also Fig. 1). The grouping of sapropels into clusters is usually straightforward, but sometimes arbitrary; their stratigraphical range and characteristics are summarised below, where "G" refers to Gibliscemi, "M" to Metochia, "K" to Kastelli, and "F" to Faneromeni (informal labeling):

cluster I is incomplete;

cluster II ranges from sapropel (of cycle) G7 to

Fig. 1. First-order and second-order correlations of the sedimentary cycles to the astronomical record: correlation of sapropel clusters to eccentricity maxima. Large-scale clusters have been correlated to 400-kyr eccentricity maxima (first-order correlations) and small-scale clusters to 100-kyr maxima (second-order correlations). The 400-kyr eccentricity cycle has been filtered from the eccentricity time series of solution La90 [1,2].

sapropel G18 (M14). No small-scale clusters could be distinguished;

cluster III ranges from sapropel G20 to sapropel G40 (M16 to M36). The presence of the thinner and less distinct sapropels G23, G28 and G32 allows the recognition of three small-scale clusters at Gibliscemi;

cluster IV ranges from sapropel G41 to sapropel G51 (M37 to M47) and contains three distinct small-scale clusters. It is separated from cluster III by a thick marlbed overlying a poorly developed sapropel (G40/M36);

cluster V ranges from sapropel G54 to sapropel G65 (M48 to M57) and similarly to cluster IV contains three small-scale clusters. At Gibliscemi, a thin sapropel (G57) is present between the lower and middle small-scale cluster which is not developed in the Metochia section (between M50 and M51). Also the upper small-scale cluster in section Gibliscemi contains an additional sapropel (G65);

cluster VI contains one typical small-scale cluster of 3 sapropels (G68–70, M58–60) and an atypical cluster which includes as many as 8 successive sapropels in the Gibliscemi and Metochia sections (G72–79, M61–68). At Gibliscemi, this atypical cluster contains an extra cycle (grey layer; G80) which is also recognised in the Kastelli section (K8). Also at Gibliscemi, a thin sapropel (G71) is found between the two clusters which is absent in Metochia (between M60 and M61). In addition, two extra thin sapropels are present in the thick homogeneous interval which separates clusters V and VI (G66 and G67). They constitute an additional small-scale cluster;

cluster VII represents an aberrant large-scale cluster. At Metochia, this cluster comprises 5 (thin) sapropels (M69–73) of which only the lowermost 3 are apparently grouped in a single small-scale cluster. But the homogeneous marl beds in between these three sapropels are twice as thick as the marl beds of cycles in the large-scale clusters VI and VIII. Hence, these cycles show a deviating pattern which is confirmed by the cycle patterns in the other sections (see Fig. 1). In contrast to Metochia and Kastelli, two extra thin sapropels (G81 and G82) are present in the thick homogeneous interval which separates clusters VII and VIII. They constitute an additional small-scale cluster;

cluster VIII is separated from cluster IX by the thick homogeneous marl bed of cycle F32 in combination with the extremely poorly-developed sapropel (i.e., grey marl bed) of cycle F33. The relatively thick homogeneous marl beds of cycles F25 and F29 allows recognition of three small-scale clusters (containing 4, 4, and 3 sapropels, respectively) in the interval ranging from sapropel F22 to F32. These small-scale clusters cannot be distinguished in the Metochia section. An extra small-scale cluster can be recognised at Kastelli (K14–16);

cluster IX is incomplete; it includes at least two small-scale clusters which contain sapropels F34–36 and grey marl beds F37–39, respectively.

Sapropels further reveal patterns which cannot be regarded as clusters. These patterns - with sapropels being alternatingly thick/thin or present/absent - are confined to specific intervals. The stratigraphic range and characteristics of these intervals are summarized below (in stratigraphic order):

sapropels G18–24 (M14–20). This interval displays a characteristic pattern which is markedly similar in the Gibliscemi and Metochia sections (Fig. 1). The homogeneous marl beds of cycles G18 (M14) and G19 (M15) are twice as thick as the marl beds of the cycles below and above. Furthermore the marl bed of cycle G18 (M14) is slightly thicker than that of cycle G19 (M15). These two extraordinary thick cycles are followed by an interval in which the well-developed and thick sapropels G20, G22 and G24 (M16, M18 and M20) alternate with the thin and poorly-developed sapropels G21 and G23 (M17 and M19), where G23 (M19) is less distinct than G21 (M17);

sapropels G49–51 (M45–47) and M58–60. These sapropels define small-scale clusters of 3 sapropels of which the middle sapropel is thinner and less prominent (Fig. 1);

sapropels G83–86 (M69–71); carbonate cycles F2–6. These cycles belong to (large-scale) cluster VII. On Gavdos, the homogeneous marl beds in between sapropels M69–71 are twice as thick as the marl beds of regular cycles below and above (Fig. 1). Hence, these cycles may represent composite ("double") cycles, i.e., cycles which contain an extra cycle that lacks sedimentary expression. This interpretation is confirmed by the sedimentary cycle patterns in the other sections. At Faneromeni, the

grey beds of the correlative cycles F2, F4 and F6 are thicker (and contain thin sand layers) than the grey beds of adjacent cycles. At Kastelli (Fig. 1), one distinct (K9) and two less distinct sapropels (K10 and K12) are separated by a thick homogeneous marl bed (between K9 and K10) and a poorly-developed grey bed (K11). Finally, an alternation of thick (G84 and G86) and thin (G83 and G85) sapropels is found just below the shearplane which marks the hiatus in the Gibliscemi section (see also [17]);

sapropels M74–78, F18–22 and K14–17 form a characteristic pattern which can be recognized all over Crete (Fig. 1). It consists of three well-developed and thick sapropels (M74, M76 and M78; F18, F20 and F22; and K14, K16 and K17) which alternate either with thin sapropels (M75 and M77) or with sedimentary cycles that lack a sapropel but contain a grey marl bed instead (F19 and F21; K15). Sapropels K16 and K17 are separated by a thick homogeneous marl bed.

3. Phase relations and astronomical solutions

The sedimentary cycle patterns described here are very similar to the patterns in the Mediterranean Plio-Pleistocene which are related to the Earth's orbital cycles of precession, eccentricity and obliquity [3,9,10,19,20]. This similarity argues for an analogous interpretation of the Miocene cycle patterns and it implies that individual sapropels are related to precession, while sapropel clusters are related to eccentricity. Deviating patterns - with sapropels being alternatingly thick/thin or present/absent - reflect interference between precession and obliquity. Similar to the Plio-Pleistocene, Miocene cycle patterns are dominantly controlled by eccentricity (sapropel clusters) and precession (individual sapropels). This astronomical interpretation of the Miocene patterns has independently been confirmed by Krijgsman et al. [15] who correlated polarity sequences of upper Miocene sections on Crete to CK92. This correlation yielded a periodicity (of 23.5 kyr) for individual sedimentary cycles which is close to the 21.7 kyr average periodicity of astronomical precession.

First results of detailed micropaleontological and geochemical studies further point to a single mechanism for sapropel formation throughout the Mediterranean Neogene [21]. We may thus safely assume that the Plio-Pleistocene phase relations between sedimentary cycles and astronomical cycles can be employed to calibrate the Miocene cycles to the astronomical record as well. As a consequence, individual sapropels of late Miocene age correspond to precession minima, small-scale sapropel clusters correspond to 100 kyr eccentricity maxima, large-scale clusters correspond to 400 kyr eccentricity maxima and "amplified" (thick) sapropels correspond to obliquity maxima [3,9].

For our calibration we have used the 65°N summer insolation curve of astronomical solution La90 [1,2] with present-day values for the dynamical ellipticity of the Earth and the tidal dissipation by the moon. We selected this target curve because it is in best agreement with sedimentary cycle patterns and orbitally controlled frequency components in climatic proxy records in the Mediterranean Pliocene–Pleistocene (see [3]). The reader is referred to the latter paper for a discussion on the selection of the La90 solution and the 65°N summer insolation curve (as target), and on the potential influence of obliquity on low latitudes.

4. Calibration to the astronomical record

The astronomical calibration of the sequence of Pliocene cycles in the Mediterranean [9,10] cannot simply be extended to the sequence of Miocene cycles because of the intervening interval of Messinian evaporites and fresh- to brackish water deposits. Hence, the astronomical calibration of the Miocene cycles is not straightforward, and several procedures can be followed to solve this problem. One procedure is to use radioisotopic age constraints from high-precision $^{40}Ar/^{39}Ar$ dating, e.g., that of chron C5n (y) at 9.67 Ma [22] or the Tortonian/Messinian boundary at 7.26 Ma [23]. We refrained from using this approach because we prefer to build an astronomical time scale that does not depend on radioisotopic dating. Another procedure would be to start from the astronomically dated Miocene/Pliocene boundary [10] and use the num-

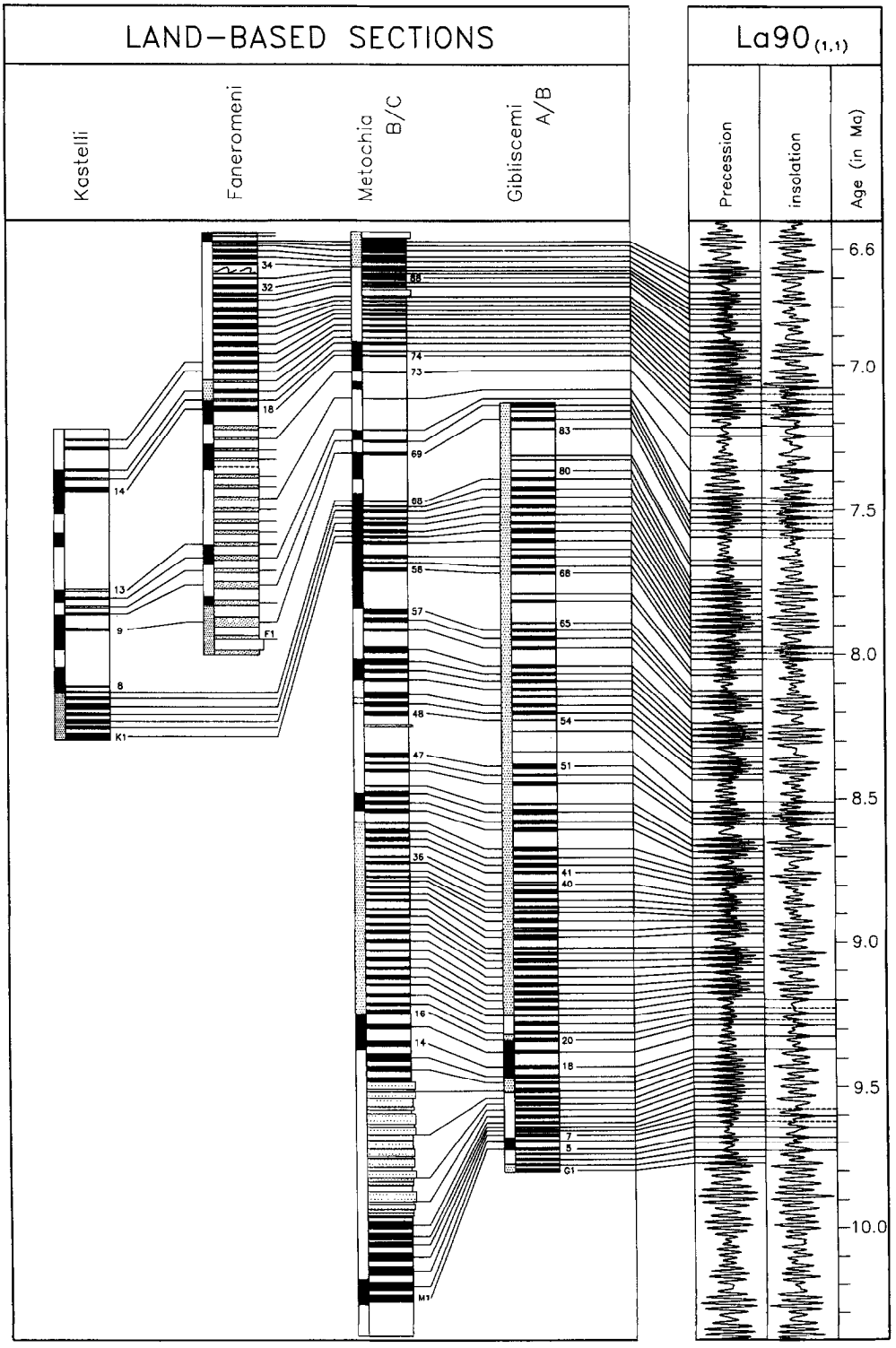
LAND–BASED SECTIONS
La90(1,1)
Kastelli
Faneromeni
Metochia B/C
Gibliscemi A/B
Precession
insolation
Age (in Ma)
6.6
7.0
7.5
8.0
8.5
9.0
9.5
10.0
34
32
18
14
13
9
8
K1
F1
74
73
69
68
58
57
48
47
36
16
14
M1
83
80
68
65
54
51
41
40
20
18
7
5
G1

ber of assumedly astronomically controlled evaporite cycles in the Mediterranean Messinian, and thus to estimate the age of the top of our upper Miocene sequence. A third procedure would be to start from the age of the youngest polarity reversal identified in our sections according to the recent geomagnetic polarity time scales CK95 and SCHPS95. Both these time scales include astronomically derived ages for reversal boundaries in the Plio-Pleistocene. We have used the last approach, but application of the other procedures would have resulted in the same astronomical calibration. We discuss this further in Section 5 (below) where we test the validity of the proposed astronomical calibration.

By using high-resolution GRAPE density and stable isotope records from ODP Leg 138 in the eastern tropical Pacific, Shackleton et al. [8] obtained a preliminary astronomical age of 6.278 Ma for C3An.2n (y). This age is 9 kyr older than the age (6.269 Ma) for the same polarity reversal in CK95. We simply added this age difference to the age of 6.567 Ma for the next older reversal in CK95 (C3An.2n (o)) to obtain a first approximation - of 6.576 Ma - for the astronomical age of the youngest polarity reversal recorded in our sections (Fig. 1, see also fig. 7 in [17]).

We then proceeded by attempting to correlate first the sapropel clusters to eccentricity. No straightforward correlation is found, however, if we use the age of 6.576 Ma for C3An.2n (o) as starting point. We then proceeded by slightly adjusting the age of this calibration point. The minimum adjustment necessary to establish a consistent correlation between sapropel clusters and eccentricity maxima is shifting the age ± 100 kyr towards older levels. The resulting correlations of large-scale sapropel clusters to 400 kyr eccentricity maxima and of small-scale clusters to 100 kyr maxima are presented in Fig. 1. The validity of these first-order and second-order correlations is supported by the position of the atypical large-scale clusters II and VII which lack a clear subdivision in small-scale clusters. These large-scale clusters correlate well with two 400-kyr eccentricity maxima at 7.4 and 9.5 Ma that lack the usually pronounced expression of the 100-kyr cycle (Fig. 1). Moreover, the large-scale clusters IV and V, which reveal the most distinct subdivision in small-scale clusters, correlate with 400-kyr eccentricity maxima, at 8.3 and 8.7 Ma, that show the most pronounced expression of the 100-kyr cycle (Fig. 1). Such variations in the expression - or "amplitude" - of the 100-kyr cycle reflect a longer-term eccentricity cycle with a period near 2 Myr. We then used the low-order correlations to establish (third-order) correlations between individual sapropels and precession minima and between individual sapropels and insolation maxima (Fig. 2). All correlations shown in Fig. 1 and 2 are internally consistent and there is still a good to excellent agreement between sapropel patterns and interference patterns of precession and obliquity back to 9.7 Ma. Only the exact calibration of the sedimentary cycles of the atypical cluster VII remains uncertain. These cycles may actually correlate with precession minima - and the corresponding insolation maxima - that are 20 to 40 kyr younger (i.e., one to two precession cycles). This alternative option implies that the unusually thick cycles F13 and F17 do not represent composite ("double") cycles, i.e., cycles which contain an extra cycle that lacks sedimentary expression, but must be considered as regular ("single") cycles.

Alternative calibrations would necessitate shifting the age of the sedimentary cycle record 400 kyr in either direction as is inherent in applying the 400 kyr eccentricity cycle for a first-order astronomical calibration. The most likely alternative calibration is by shifting the cycle record 400 kyr towards younger levels which would imply a 300 kyr ($= 400 - 100$) adjustment of our initial age of 6.576 Ma for C3An.2n (o). We superficially explored this alternative calibration and a very limited number of other alternatives. All these exercises resulted in correlations which are not convincing and less consistent than the correlations presented in Fig. 1 and 2. Summarizing,

Fig. 2. Third-order correlations of the individual sedimentary cycles to precession minima and of alternatingly thick/thin sapropels/cycles to interference patterns of precession and obliquity as reflected in the 65°N summer insolation curve of solution La90 with present-day values for the dynamical ellipticity of the Earth and tidal dissipation by the moon ($La90_{(1,1)}$, see [3]).

Table 1
Comparison of the astronomical ages of reversal boundaries with the ages of the corresponding reversals in recently advanced polarity time scales of Cande and Kent ([18], CK95) and Shackleton et al. ([8], SCHPS95)

reversal	ref. [3]/ this paper	CK95	Δ	SBP90/ SCHPS95	Δ
C1n		0.780		0.780	
C1r.1n (y)		0.990		0.990	
C1r.1n (o)		1.070		1.070	
C2n (y)	**1.785**	1.770	*0.015*	1.770	*0.015*
C2n (o)	**1.942**	1.950	*-0.008*	1.950	*-0.008*
C2r.1n (y)	**2.129**	2.140	*-0.011*		
C2r.1n (o)	**2.149**	2.150	*-0.001*		
C2An.1n (y)	**2.582**	2.600	*-0.018*	2.600	*-0.018*
C2An.1n (o)	**3.032**	3.040	*-0.008*	3.046	*-0.014*
C2An.2n (y)	**3.116**	3.110	*0.006*	3.131	*-0.015*
C2An.2n (o)	**3.207**	3.220	*-0.013*	3.233	*-0.026*
C2An.3n (y)	**3.330**	3.330	*0.000*	3.331	*-0.001*
C2An.3n (o)	**3.596**	3.580	*0.016*	3.594	*0.002*
C3n.1n (y)	**4.188**	4.180	*0.008*	4.199	*-0.011*
C3n.1n (o)	**4.300**	4.290	*0.010*	4.316	*-0.016*
C3n.2n (y)	**4.493**	4.480	*0.013*	4.479	*0.014*
C3n.2n (o)	**4.632**	4.620	*0.012*	4.623	*0.009*
C3n.3n (y)	**4.799**	4.800	*-0.001*	4.781	*0.018*
C3n.3n (o)	**4.896**	4.890	*0.006*	4.878	*0.018*
C3n.4n (y)	**4.998**	4.980	*0.018*	4.977	*0.021*
C3n.4n (o)	**5.236**	5.230	*0.006*	5.232	*0.004*
C3An.1n (y)	*5.952*	5.894	*0.059*	5.875	*0.077*
C3An.1n (o)	*6.214*	6.137	*0.079*	6.122	*0.092*
C3An.2n (y)	*6.356*	6.269	*0.089*	6.256	*0.100*
C3An.2n (o)	**6.677**	6.567	*0.110*	6.555	*0.122*
C3Bn (y)	**7.101**	6.935	*0.166*	6.919	*0.182*
C3Bn (o)	**7.210**	7.091	*0.119*	7.072	*0.138*
C3Br.1n (y)	**7.256**	7.135	*0.121*		
C3Br.1n (o)	**7.301**	7.170	*0.131*		
C3Br.2n (y)	**7.455**	7.341	*0.114*		
C3Br.2n (o)	**7.492**	7.375	*0.117*		
C4n.1n (y)	**7.532**	7.432	*0.100*	7.406	*0.126*
C4n.1n (o)	**7.644**	7.562	*0.082*	7.533	*0.111*
C4n.2n (y)	**7.697**	7.650	*0.047*	7.618	*0.079*
C4n.2n (o)	**8.109**	8.072	*0.037*	8.027	*0.082*
C4r.1n (y)	**8.257**	8.225	*0.032*	8.174	*0.083*
C4r.1n (o)	**8.303**	8.257	*0.046*	8.205	*0.098*
C4r.2r-1 (y)	**8.659**	8.635	*0.024*		
C4r.2r-1 (o)	**8.702**	8.651	*0.051*		
C4An (y)	*8.750*	8.699	*0.051*	8.631	*0.119*
C4An (o)	*9.075*	9.025	*0.050*	8.945	*0.130*
C4Ar.1n (y)	**9.280**	9.230	*0.050*	9.142	*0.138*
C4Ar.1n (o)	**9.377**	9.308	*0.069*	9.218	*0.159*
C4Ar.2n (y)	**9.629**	9.580	*0.049*	9.482	*0.147*
C4Ar.2n (o)	**9.679**	9.642	*0.037*	9.543	*0.136*
C5n.1n (y)		9.740		9.639	

we are convinced that the proposed astronomical calibration is essentially correct and that it is based on continuous sedimentary successions.

The calibration of the sedimentary cycle record to precession and summer insolation (Fig. 2) was used to establish an astronomical time scale for the late Miocene. It results in ages for the individual sedimentary cycles, and hence for all biostratigraphic datum planes and polarity reversals in our sections (see Appendices A and B). The age of the Tortonian/Messinian boundary placed at the level of the first regular occurrence of the *Globorotalia conomiozea* group is estimated at 7.24 Ma. Since the age of the Miocene/Pliocene boundary is 5.33 Ma [3], the duration of the Messinian is 1.91 Myr. Note that the alternative option for the astronomical calibration of the sedimentary cycles in large-scale cluster VII (see above) results in slightly younger ages for all reversals and bioevents between 7.6 and 7.2 Ma. According to this option, the age of the T/M boundary is 7.21 Ma and the duration of the Messinian 1.88 Myr.

The exact accuracy of astronomical solutions and hence of our astronomical ages is difficult to determine [24,25] also because other factors, i.e., the tidal dissipation by the moon and the dynamical ellipticity of the Earth, which are influenced by glacial cycles, start to play a role [2]. The analytical solution La90 is in excellent agreement with the numerical solution QTD90 [25] once the same term for the tidal dissipation is introduced. The latter solution is supposedly very accurate [25], but was not computed for time intervals older than 3 million years. Also the excel-

Notes to Table 1:
Ages of reversals which could not be dated directly because of their late Messinian age or of poor magnetostratigraphic results in our sections have been obtained by linear interpolation of seafloor-spreading rates between the nearest younger and older astronomically-dated reversals in the synthetic anomaly profile of Cande and Kent [16]: these ages are shown in italics. Ages of younger polarity reversals -of Plio-Pleistocene age -have been included. They are taken from Cande and Kent ([18], CK95), Shackleton et al. ([7], SBP90; [8], SCHPS95) and Lourens et al. [3]. Cande and Kent [18] included astronomical ages of Shackleton et al. [7] and Hilgen [10] for this time interval. In the present paper, the same astronomical solution and target curve is used as the one preferred by Lourens et al. [3].

lent agreement with sedimentary cycle patterns in the Mediterranean Pliocene suggests that the selected target curve -$La90_{(1,1)}$ summer insolation - is very accurate [3]. The error in the astronomical ages can roughly be estimated to be in the order of 5 kyr at 5.0 Ma. This error may well increase to 10–20 kyr around 10.0 Ma.

Our astronomical ages of the polarity reversals are invariably older than the ages in recent polarity time scales (Table 1). It is remarkable that the discrepancies with CK95 are largest for the youngest reversals dated (up to 166 kyr) and decrease gradually to values between 25 and 70 kyr for older reversals. Discrepancies with SCHPS95 further indicate that our astronomical calibration is not in agreement with the preliminary and partial astronomical tuning of GRAPE records from ODP leg 138 for the interval between 6.0 and 10.0 Ma [8]. Unpublished work on ODP leg 154 sediments (Shackleton, pers. commun., 1995) also shows that the late Miocene age estimates of Shackleton et al. [8] are too young.

5. Testing the validity of the astronomical calibration

In this chapter, we attempt to test the validity of the new time scale. Independent tests must either come from astronomical calibration of other, preferably extra-Mediterranean records or from high-precision radioisotopic dating. In addition, the number of sedimentary cycles in the remaining younger part of the Mediterranean Messinian may provide important constraints.

5.1. Radioisotopic age constraints

The time scale can be tested by comparing astronomical ages of polarity reversals or biostratigraphic datum planes with radioisotopic age constraints for the same events. Recent radioisotopic results include an age of 9.51 Ma for chron C4Ar.2n (o) [22] and an age of 7.07 Ma for the Tortonian/Messinian boundary [26]. We did not include K/Ar ages (e.g., from Iceland [27]) because radioisotopic dating of lavas often yield ages that are too young. We have sampled ashbeds that are intercalated in the Metochia section and in parallel sections on Crete (e.g., Faneromeni, Kastelli) for Ar/Ar dating, but the results are not yet available.

Baksi et al. [22] carried out $^{40}Ar/^{39}Ar$ incremental heating studies on whole rock basalts of a number of lava flows from Akaroa Volcano, New Zealand. These lava flows span two successive field reversals. The lower normal to reversed (N–R) transition is assumed to represent the termination of chron C5. This boundary was previously dated at 8.9 Ma by Evans [28] who used the K/Ar method. The new results yielded a weighted mean plateau age of 9.67 $\pm$ 0.05 Ma for this boundary, while the younger (R–N) reversal was dated at 9.51 $\pm$ 0.05 Ma. The latter age is slightly younger than our astronomical age of 9.66 Ma for the same reversal. Although Berggren et al. [29] point out that the lower transition at Akaroa can also be correlated with either chron C5n.1r/C5n.2n or chron C4Ar.2r/n boundary, any other option than the one preferred by Evans [28] and Baksi et al. [22] would increase the discrepancy with the astronomical age for C4Ar.2n (o).

Using K/Ar dating on biotite and a single Ar/Ar dating on plagioclase, Vai et al. [23] dated several volcanogenic beds intercalated in upper Tortonian–lower Messinian marine sequences in the northern Apennines. They obtained an age of 7.26 Ma for the Tortonian/Messinian boundary through linear extrapolation of the sedimentation rate over a short distance. Recently, Vai and Laurenzi [26] provided a series of additional Ar/Ar datings of biotite-rich ash layers spanning the Tortonian/Messinian boundary in the Monte del Casino section. They arrived at a revised age of 7.07 $\pm$ 0.05 Ma for the boundary which is younger than their previous estimate of 7.26 Ma and also younger than our astronomical age of 7.24 Ma.

A straightforward comparison between the radiometric and astronomical ages, however, should be viewed with caution because of the age uncertainty of fluence monitor standards in radioisotopic dating. For example, the age of the Fish Canyon Tuff (FCT), which provides one of the most widely used standards for age calibration in radioisotopic dating, varies between 27.55 and 27.95 Ma [14,22,30]. This age uncertainty results in a potential error of 1.5%. To eliminate this uncertainty, Renne et al. [14] compared Ar/Ar ages with astronomical ages for seven

Table 2
Comparison of astronomical and Ar/Ar ages for C4Ar.2n (o) and the Tortonian–Messinian boundary

datum	radiometric age	FCT age 27.95	FCT age 28.03	astronomical age
T/M boundary	7.07 ± 0.05	7.17	7.19	**7.240**
C4Ar.2n (y)	9.51 ± 0.05	9.51	9.54	**9.679**

Ar/Ar ages have been recalculated to ages of 27.95 and 28.03 Ma for the Fish Canyon Tuff sanidine following the formula given in Dalrymple et al. [40].

polarity reversals over the last 3.5 Myrs and they derived a best age estimate of 27.95 (or 28.03) Ma for the FCT sanidine.

Baksi et al. [22] used an age of 27.95 Ma for Fish Canyon Tuff biotite whereas Vai et al. [23] and Vai and Laurenzi [26] used 27.55 Ma. In Table 2, we compared the Ar/Ar ages of both C4Ar.2n (o) and the Tortonian/Messinian boundary - recalculated to ages of 27.95 and 28.03 Ma for the Fish Canyon Tuff - with the astronomical ages. This comparison shows that the Ar/Ar ages are now in better agreement with the astronomical ages. In particular, they support our preferred astronomical calibration because they are totally inconsistent with ages that are 400 kyr younger (or older) than our astronomical ages. The age difference for the T/M boundary is further reduced considering that Vai and Laurenzi [26] equate the boundary with a level *above* the first regular occurrence (FRO) of the *G. conomiozea* group (i.e., the first occurrence level of *G. conomiozea* types), whereas we use the FRO level of the *G. conomiozea* group (see [17]). The use of the alternative option to astronomically calibrate the sed-

Table 3
Number of sedimentary cycles per stratigraphic unit and per evaporite basin

lithostrat. unit	Calt.	Cim.	V.Ges.	R.-M.	Gavd.	**comp.**	**astr.**
Upper evaporites	7-8	6-8		6-8		**8**	
Intermediate marls		1				**1**	
Lower evaporites		15/16	16	15		**16**	
Calcare di Base	*4-13*	4	4 (±2)			**4 (±2)**	
Tripoli diatomites	*>34*				38	**38**	
total no. cycles						**67 (±2)**	**67**

For the Ciminna Basin, we included both the "lower selenite gysum" and the "laminated gypsum" of Bommarito and Catalano [32] in the Lower Evaporites. In that case, the transition from "lower selenite" to "laminated gypsum" would correspond with the transition from major (thicker) to minor (thinner) evaporite cycles in the Vena del Gesso Basin (see [34]) and the major discontinuity in the evaporite sequences would invariably separate the Lower from the Upper Evaporites. In the Romagna–Marche basin, the Upper Evaporites do not exhibit the usual gypsum-bearing cycles but consist of a cyclic alternation of thin evaporitic limestone beds and marly clays of the Colombacci Formation.

In the total number count of the sedimentary cycles, we preferred to use the 38 diatomite cycles from Gavdos because they are tectonically less disturbed than the diatomites in the Falconara section. Moreover, they are in stratigraphic continuity with our Metochia section, thus excluding discrepancies as a consequence of a diachronous base of the diatomites (e.g. [36]). The large numbers of 6–9 and 4–13 cycles of the Calcare di Base in the Caltanissetta Basin as reported by Pedley and Grasso [41] and Decima et al. [42] have not been used because these cycles represent at least partly the lateral (= marginal) equivalent of the lower evaporites and/or the top of the Tripoli diatomites (see [43]).

imentary cycles of large-scale cluster VII (see Section 4, above) results in a reduction of this discrepancy as well.

5.2. *Cyclostratigraphic framework of Messinian evaporites*

Cyclic bedding is not restricted to the pre-evaporitic part of the Mediterranean Messinian, since the evaporites often show a pronounced cyclic bedding as well. Here, we investigate whether the number of sedimentary cycles in the younger part of the Mediterranean Messinian is consistent with what we might expect from the astronomical calibrations.

The standard succession of the Messinian evaporites comes from the Caltanissetta Basin on Sicily [31]. In stratigraphical order, this succession includes diatomites of the Tripoli Formation, partly evaporitic limestones of the Calcare di Base, massive gypsum and halite of the Lower Evaporites, gypsum arenites, and selenitic gypsum of the Upper Evaporites. All units except the Tripoli diatomites belong to the Gessoso–Solfifera Formation. Because no literature data are presently available on the number of cycles for all units, we included information from Gavdos and from basins other than the Caltanissetta Basin, in particular the Ciminna Basin on northern Sicily [32] and the Vena del Gesso and Romagna–Marche Basins in the northern Apennines [33–35].

The number of sedimentary cycles has been summarised per stratigraphic unit and per basin in Table 3. The consistent number of evaporite cycles in all basins suggests that disturbing effects of hiatuses on the continuity of the evaporite sequences is small. Also, the disturbing effect of lateral facies changes will be small because most of the cyclically bedded sequences have been logged in stratigraphic succession.

The best current estimate for the total number of sedimentary cycles in our composite evaporite sequence of the Mediterranean Messinian, including the pre-evaporitic diatomites, is 67 ± 2. For the composite, we preferred to use the 38 diatomite cycles from Gavdos because they are tectonically less disturbed than the diatomites in the Falconara section. Moreover, they are in stratigraphic continuity with our Metochia section, thus excluding discrepancies as a consequence of a diachronous base of the diatomites (e.g., [36]). Here, we assume that all cycles are related to precession. This assumption is based on - both observed as well as inferred - lithological relationships between the different types of sedimentary cycles ([33], authors' field observations). Field observations for instance clearly reveal that sapropels pass into diatomites of the Tripoli Formation and that the diatomite cycles are replaced by cycles of the Calcare di Base.

The number of 67 can now be compared with the number of precession cycles in the same time interval, i.e., between the base of the diatomites, dated astronomically at 6.70 Ma, and the Miocene/Pliocene boundary, dated at 5.33 Ma. This interval contains 67 precession cycles. This number is in excellent agreement with our estimate of 67 ± 2 for the total number of sedimentary cycles even though the exact number remains uncertain. Using this preliminary cyclostratigraphic framework, we obtained ages of 5.95 Ma for the base of the Calcare di Base, and of 5.87 and 5.52 Ma for the base of the Lower Evaporites and Upper Evaporites, respectively.

Our framework differs from that of Vai [35] by the larger number of sedimentary cycles in the pre-evaporitic Messinian, and in that we held precession rather than obliquity responsible for the formation of cycles in the Upper Evaporites. Evidence for the precessional forcing of these cycles comes from Ar/Ar ages of 5.4 ± 0.06 and 5.5 ± 0.05 Ma for an ash layer intercalated directly below the first limestone (''Colombaccio'') marker bed in the northern Apennines (Odin, 1995, as referred to by Vai [35]). These ages are in good agreement with our age of 5.52 Ma for the base of the Upper Evaporites, but they are too young in case the Upper Evaporite cycles are obliquity controlled.

Another consequence of our framework is that the onset of evaporite formation is younger than 6.0 Ma and even postdates the Gilbert/Chron 5 boundary tentatively dated at 5.953 Ma (see Table 1). This outcome is in agreement with Gautier et al. [37] who, based on the magnetostratigraphy of the Sorbas section in Spain, placed the onset of evaporite formation in the early Gilbert as well. This onset now closely coincides with the most extreme glacial stages TG 20 and 22 in the high-resolution stable isotope records of ODP Site 846 from the equatorial Pacific [38] and Atlantic Morocco [39] suggesting at least a partial

glacio-eustatic control on the final isolation of the Mediterranean during the latest Miocene.

6. Conclusions

Marine sequences exposed in Mediteranean land-based sections allow the construction of an astronomical time scale for the late Miocene by correlating characteristic sedimentary cycle patterns to target curves of astronomical solution La90 with present-day values for the dynamical ellipticity of the Earth and the tidal dissipation by the moon. This correlation yields ages for the individual sedimentary cycles, and for the polarity reversals and planktonic foraminiferal and dinoflagellate events recorded. The Tortonian/Messinian boundary is dated at 7.24 Ma (or 7.21 Ma).

Astronomical ages of the polarity reversals are older (up to 182 kyr) than the ages of the corresponding reversals in the most recent geomagnetic polarity time scales of CK95 and SCHPS95. Discrepancies with CK95 are largest for the youngest reversals dated (up to 166 kyr) and decrease gradually to values between 25 and 70 kyr for older reversals. Discrepancies with SCHPS95 indicate that our calibration is not in agreement with the preliminary and partial astronomical tuning of GRAPE records from ODP leg 138 for the interval between 6.0 and 10.0 Ma [8].

The new time scale is consistent with recent $^{40}Ar/^{39}Ar$ ages of volcanic beds and with the number of sedimentary cycles in the younger partly evaporitic part of the Mediterranean Messinian.

Acknowledgements

Two anonymous reviewers are thanked for their critical comments. This study was partly supported by the Netherlands Geosciences Foundation (GOA) with financial aid from the Netherlands Organization of Scientific Research (NWO) and the EU HCM program. This is MIOMAR project contribution No. 4. [*RV*,*MK*]

Appendix A

Astronomical ages of individual sedimentary cycles. Ages refer to the mid-points of sapropels and/or grey layers and represent 3-kyr lagged ages of the correlative precession minima (p) or the summer insolation maxima (i) based on the third-order correlations of the sedimentary cycles to the astronomical record shown in Fig. 2. The 3-kyr lag is based on the difference in age between the youngest Holocene sapropel in the Mediterranean and the correlative precession minimum/insolation maximum (see [3]).

Sedimentary cycle				age 1	age 2	Cycle			age 1	age 2	Cycle		age 1	age 2
Kas	Gib	Met	Fan	p	i	Kas	Gib	Met	p	i	Gib	Met	p	i
		M96	F39	6.654	6.654		G81		7.694	7.693	G40	M36	8.829	8.829
		M95	F38	6.675	6.675	K8	G80		7.743	7.743	G39	M35	8.849	8.849
		M94	F37	6.696	6.696	K7	G79	M68	7.766	7.766	G38	M34	8.869	8.869
		M93	F36	6.748	6.749	K6	G78	M67	7.787	7.787	G37	M33	8.889	8.889
		M92	F35	6.769	6.768	K5	G77	M66	7.809	7.808	G36	M32	8.904	8.905
		M91	F34	6.789	6.789	K4	G76	M65	7.833	7.834	G35	M31	8.923	8.923
		M90	F33	6.808	6.807	K3	G75	M64	7.858	7.857	G34	M30	8.944	8.944
		M89		6.825	6.826	K2	G74	M63	7.880	7.880	G33	M29	8.965	8.965
		M88	F32	6.845	6.844	K1	G73	M62	7.901	7.901	G32	M28	9.015	9.015
		M87	F31	6.865	6.866		G72	M61	7.923	7.923	G31	M27	9.037	9.037
		M86	F30	6.886	6.884		G71		7.950	7.950	G30	M26	9.058	9.058
		M85	F29	6.917	6.917		G70	M60	7.973	7.973	G29	M25	9.080	9.080
		M84	F28	6.938	6.938		G69	M59	7.994	7.994	G28	M24	9.104	9.105
		M83	F27	6.960	6.960		G68	M58	8.015	8.015	G27	M23	9.130	9.129
		M82	F26	6.982	6.982		G67		8.051	8.051	G26	M22	9.151	9.152
		M81	F25	7.008	7.005		G66		8.070	8.069	G25	M21	9.173	9.172
		M80	F24	7.031	7.032		G65		8.125	8.125	G24	M20	9.195	9.195
K18		M79	F23	7.053	7.052		G64	M57	8.145	8.144	G23	M19	9.222	9.225
K17		M78	F22	7.074	7.075		G63	M56	8.165	8.165	G22	M18	9.246	9.245
		M77	F21	7.097	7.097		G62	M55	8.186	8.186	G21	M17	9.266	9.267
K16		M76	F20	7.123	7.123		G61	M54	8.237	8.236	G20	M16	9.285	9.284
K15		M75	F19	7.146	7.146		G60	M53	8.258	8.258	G19	M15	9.322	9.322
K14		M74	F18	7.167	7.167		G59	M52	8.279	8.279	G18	M14	9.368	9.367
			F17	7.212	7.207		G58	M51	8.300	8.300	G17	M13	9.393	9.394
		M73	F16	7.242	7.242		G57		8.322	8.323	G16	M12	9.415	9.414
			F15	7.262	7.263		G56	M50	8.352	8.351	G15	M11	9.437	9.438
			F14	7.280	7.280		G55	M49	8.373	8.373	G14	M10	9.461	9.460
			F13	7.316	7.317		G54	M48	8.394	8.393	G13	M9	9.484	9.484
			F12	7.339	7.338		G53		8.433	8.432	G12	M8	9.507	9.507
		M72	F11	7.361	7.361		G52		8.507	8.507	G11	M7	9.529	9.528
			F10	7.385	7.386		G51	M47	8.545	8.545	G10	M6	9.552	9.554
			F9	7.409	7.408		G50	M46	8.565	8.566	G9	M5	9.577	9.576
			F8	7.431	7.431		G49	M45	8.587	8.586	G8	M4	9.599	9.600
K13			F7	7.454	7.453		G48	M44	8.638	8.638	G7	M3	9.621	9.619
K12		M71	F6	7.477	7.478		G47	M43	8.659	8.659	G6	M2	9.641	9.642
K11			F5	7.500	7.500		G46	M42	8.680	8.680	G5	M1?	9.676	9.677
K10	G86	M70	F4	7.523	7.523		G45	M41	8.702	8.702	G4		9.697	9.696
	G85		F3	7.545	7.545		G44	M40	8.731	8.732	G3		9.725	9.724
K9	G84	M69	F2	7.569	7.567		G43	M39	8.753	8.753	G2		9.748	9.749
	G83		F1	7.593	7.594		G42	M38	8.774	8.774	G1		9.770	9.770
	G82			7.673	7.674		G41	M37	8.794	8.794				

Appendix B

Astronomical ages of biostratigraphic datum planes and polarity reversals. Ages have been obtained by linear interpolation of the sedimentation rate between astronomically-dated calibration points shown in Appendix A. We used the 3-kyr lagged ages of insolation maxima for the sapropels as starting point.

		Gibliscemi	Metochia	Kastelli	Faneromeni	range	chron	age
magnetic reversal								
C3An.2n (o)					6.675-6.678	6.675-6.678		**6.677**
C3Bn (y)			*7.106-7.133*	7.094-7.108	-	7.094-7.108		**7.101**
C3Bn (o)			*7.216-7.223*	*7.208-7.214*	7.203-7.218	7.203-7.218		**7.210**
C3Br.1n (y)			*7.257-7.268*	*7.255-7.262*	7.249-7.264	7.249-7.264		**7.256**
C3Br.1n (o)			*7.301-7.316*	*7.296-7.302*	7.299-7.304	7.299-7.304		**7.301**
C3Br.2n (y)			*7.474-7.478*	7.455-7.462	7.452-7.455	7.455		**7.455**
C3Br.2n (o)			*7.517-7.522*	7.488-7.496	7.480-7.499	7.488-7.496		**7.492**
C4n.1n (y)			*7.545-7.552*	7.519-7.536	7.529-7.535	7.529-7.535		**7.532**
C4n.1n (o)			*7.649-7.678*	7.639-7.649		7.639-7.649		**7.644**
C4n.2n (y)			*7.695-7.742*	7.692-7.703		7.692-7.703		**7.697**
C4n.2n (o)			8.102-8.116			8.102-8.116		**8.109**
C4r.1n (y)			8.247-8.267			8.247-8.267		**8.257**
C4r.1n (o)			8.296-8.310			8.296-8.310		**8.303**
C4r.2r-1 (y)			8.648-8.670			8.648-8.670		**8.659**
C4r.2r-1 (o)			8.694-8.710			8.694-8.710		**8.702**
C4An (y)			-					-
C4An (o)			-					-
C4Ar.1n (y)		9.256-9.304	-			9.256-9.304		**9.280**
C4Ar.1n (o)		*9.384-9.430*	9.376-9.378			9.376-9.378		**9.377**
C4Ar.2n (y)		9.627-9.642	9.628-9.630			9.628-9.630		**9.629**
C4Ar.2n (o)		9.675-9.684	*9.696-9.714*			9.675-9.684		**9.679**
planktonic foram	**event**							
11) *G. nicolae*	FO		6.826-6.831		6.822-6.831	6.826-6.831	**C3Ar**	**6.829**
10) *G. conomiozea gr.*	FRO		7.237-7.241	*7.239-7.249*	7.240-7.243	7.240-7.241	**C3Br.1r**	**7.240**
9) *G. menardii 5*	FO		7.353-7.356	*7.351-7.356*	7.353-7.359	7.353-7.356	**C3Br.2r**	**7.355**
8) *C. parvulus*	LO		7.446-7.466	-	-	7.446-7.466	**C3Br.2r**	**7.456**
7) *G. menardii 4*	LCO		7.507-7.512	7.512-7.519	7.511-7.519	7.512	**C3Br.3r**	**7.512**
6) *S. seminulina*	hro	7.719-7.727	7.720-7.731	7.724-7.729		7.724-7.727	**C4n.2n**	**7.726**
5) *S. seminulina*	lro	7.913-7.921	7.915-7.921			7.915-7.921	**C4n.2n**	**7.918**
4) *C. parvulus*	fs	8.420-8.429	8.420-8.442			8.420-8.429	**C4r.2r**	**8.425**
3) *C. parvulus (ls)*	LCO	8.869-8.872	8.863-8.868			8.863-8.868	-	**8.865**
2) *G. menardii 4*	lco	9.309-9.316	9.312-9.324			9.312-9.316	**C4Ar.1n(y)**	**9.314**
1) *N. acostaensis dex*	hro	9.531-9.541	9.546-9.549			9.546-9.549	**C4Ar.2r**	**9.548**
II) *G. conomiozea gr.*	FO	7.890-7.893	*7.863-7.867*	*7.864-7.869*		7.890-7.893	**C4n.2n**	**7.892**
I) *G. dehiscens*	influx	8.969-8.990	8.970-8.984			8.970-8.984	-	**8.977**
dinoflagellate								
i) *L. truncatum*	LO	7.789-7.800				7.789-7.800	**C4n.2n**	**7.795**
h) *T. psilatum*	LCO	8.003-8.041				8.003-8.041	**C4n.2n**	**8.022**
g) *C? labradorii*	LO	8.061-8.077				8.061-8.077	**C4n.2n**	**8.069**
f) *M. sp. A*	LO	8.197-8.243				8.197-8.243	**C4r.1r**	**8.220**
e) *C? labradorii*	FO	8.289-8.312				8.289-8.312	**C4r.2r/C4r.1n**	**8.300**
d) *P. golzowense*	LO	8.762-8.785				8.762-8.785	-	**8.774**
c) *I. maculatum*	FO	9.260-9.272				9.260-9.272	**C4Ar.1r**	**9.266**
b) *M. sp. A*	LCO	9.435-9.452				9.435-9.452	**C4Ar.2r**	**9.444**
a) *C. sp. A*	LO	9.586-9.614				9.586-9.614	**C4Ar.2r**	**9.600**

References

[1] J. Laskar, The chaotic motion of the solar system: a numerical estimate of the size of the chaotic zones, Icarus 88, 266–291, 1990.

[2] J. Laskar, F. Joutel and F. Boudin, Orbital, precessional, and insolation quantities for the Earth from −20 Myr to +10 Myr, Astron. Astrophys. 270, 522–533, 1993.

[3] L.J. Lourens, A. Antonarakou, F.J. Hilgen, A.A.M. Van Hoof, C. Vergnaud-Grazzini and W.J. Zachariasse, Evaluation of the Plio-Pleistocene astronomical time scale, Paleoceanography, in press.

[4] C. Emiliani, Paleotemperature analysis of the Caribbean cores P6304-8 and P6304-9 and a generalized temperature curve for the last 425,000 years, J. Geol. 63, 538–578, 1966.

[5] N.J. Shackleton and N.D. Opdyke, Oxygen isotope and paleomagnetic stratigraphy of Pacific core V28-238: oxygen isotope temperatures and ice volumes on a 10^5 and 10^6 year scale, Quat. Res. 3, 39–55, 1973.

[6] J.D. Hays, J. Imbrie and N.J. Shackleton, Variations in the Earth's orbit: Pacemaker of the ice ages, Science 194, 1121–1132, 1976.

[7] N.J. Shackleton, A. Berger and W.R. Peltier, An alternative astronomical calibration of the lower Pleistocene time scale based on ODP site 677, Trans. R. Soc. Edinburgh 81, 251–261, 1990.

[8] N.J. Shackleton, S. Crowhurst, T. Hagelberg, N.G. Pisias and D.A. Schneider, A new late Neogene time scale: Application to leg 138 sites, Proc. ODP Sci. Results 138, in press, 1995.

[9] F.J. Hilgen, Astronomical calibration of Gauss to Matayama sapropels in the Mediterranean and implication for the Geomagnetic Polarity Time Scale, Earth Planet. Sci. Lett. 104, 226–244, 1991.

[10] F.J. Hilgen, Extension of the astronomically calibrated (polarity) time scale to the Miocene/Pliocene boundary, Earth Planet, Sci. Lett. 107, 349–368, 1991.

[11] R. Tiedemann, M. Sarnthein and N.J. Shackleton, Astronomic timescale for the Pliocene Atlantic $\delta^{18}O$ and dust flux records of Ocean Drilling Program site 659, Paleoceanography 9, 619–638, 1994.

[12] L.J. Lourens, F.J. Hilgen, L. Gudjonsson and W.J. Zachariasse, Late Pliocene to early Pleistocene astronomically forced sea surface productivity and temperature variations in the Mediterranean, Mar. Micropaleontol. 19, 49–78, 1992.

[13] D.S. Wilson, Confirmation of the astronomical calibration of the magnetic polarity timescale from sea-floor spreading rate, Nature 364, 788–790, 1993.

[14] P.R. Renne, A.L. Deino, R.C. Walter, B.D. Turrin, C.C. Swisher, T.A. Becker, G.H. Curtis, W.D. Sharp and A.-R. Jaouni, Intercalibration of astronomical and radioisotopic time, Geology 22, 783–786, 1994.

[15] W. Krijgsman, F.J. Hilgen, C.G. Langereis and W.J. Zachariasse, The age of the Tortonian/Messinian boundary, Earth Planet. Sci. Lett. 121, 533–547, 1994.

[16] S.C. Cande and Kent, D.V., A New Geomagnetic Polarity Time Scale for the Late Cretaceous and Cenozoic, J. Geophys. Res. 97, 13,917–13,951, 1992.

[17] W. Krijgsman, F.J. Hilgen, C.G. Langereis, A. Santarelli and W.J. Zachariasse, Late Miocene magnetostratigraphy, biostratigraphy and cyclostratigraphy from the Mediterranean, Earth Planet. Sci. Lett. 136, this issue.

[18] S.C. Cande and Kent, D.V., Revised calibration of the Geomagnetic Polarity Time Scale for the Late Cretaceous and Cenozoic, J. Geophys. Res. 100, 6093–6095, 1995.

[19] M. Rossignol-Strick, Mediterranean Quaternary sapropels, an immediate climatic response to orbital insolation, Nature 303, 46–49, 1983.

[20] F.J. Hilgen, Sedimentary rhythms and high-resolution chronostratigraphic correlations in the Mediterranean Pliocene, Newslett. Stratigr. 17, 109–127, 1987.

[21] I.A. Nijenhuis and S.J. Schenau, The origin of some Miocene sapropelites of Faneromeni, Crete. A geo-chemical survey, Intern. Rep., Dep. Geochem. Inst. Earth Sciences, Utrecht Univ., Utrecht, 1995.

[22] A.K. Baksi, K.A. Hoffman and E. Farrar, A new calibration point for the late Miocene section of the geomagnetic polarity time scale: $^{40}Ar/^{39}Ar$ dating of lava flows from Akaroa volcano, New Zealand, Geophys. Res. Lett. 20, 667–670, 1993.

[23] G.B. Vai, I.M. Villa and M.L. Colalongo, First radiometric dating of the Tortonian/Messinian boundary, C.R. Acad. Sci. Paris 316, 1407–1414, 1993.

[24] A. Berger and M.F. Loutre, Astronomical solutions for paleoclimatic studies over the last 3 million years, Earth Planet. Sci. Lett. 111, 369–382.

[25] T.R. Quinn, S. Tremaine and M. Duncan, A three million year integration of the Earth's orbit, Astron. J. 101, 2287–2305, 1991.

[26] G.B. Vai and M. Laurenzi, Radiometric dating of the Tortonian/Messinian boundary (N. Apennines, Italy), in: 8th Conf. Geochron. Cosmochron. Isot. Geol., Berkeley, USGS Circ. 1107, 133, 1994.

[27] I. McDougall, L. Kristjansson and K. Saemundsson, Magnetostratigraphy and geochronology of northwest Iceland, J. Geophys. Res. 89, 7029–7060, 1984.

[28] A.L. Evans, Geomagnetic polarity reversals in a Late Tertiary lava sequence from Akaroa Volcano, New Zealand, Geophys. J.R. Astron. Soc. 21, 163–183, 1970.

[29] W.A. Berggren, D.V. Kent, C.C. Swisher and M.-P. Aubry, A revised Cenozoic geochronology and chrono-stratigraphy, in: Geochronology, Time Scales and Global Stratigraphic Correlations: A Unified Temporal Framework for a Historical Geology, W.A. Berggren, D.V. Kent and J. Hardenbol, eds., SEPM Spec. Vol., in press.

[30] G.A. Izett, G.B. Dalrymple and L.W. Snee, $^{40}Ar/^{39}Ar$ age of the Cretaceous–Tertiary boundary tektites from Haïti, Science 252, 1539–1542, 1991.

[31] A. Decima and F.C. Wezel, Late Miocene evaporites of the central Sicilian Basin, Init. Rep. DSDP 13, 1234–1240, 1973.

[32] S. Bommarito and R. Catalano, Facies analysis of an evaporitic Messinian sequence near Ciminna (Palermo, Sicily), in: Messinian Events in the Mediterranean, C.W. Drooger, ed., pp. 172–177, North Holland, Amsterdam, 1973.

[33] G.B. Vai and F. Ricci Lucchi, The Vena del Gesso in northern Apennines: growth and mechanical breakdown of gypsified algal crusts, Mem. Soc. Geol. Ital. 16, 217–249, 1976.

[34] G.B. Vai, A field trip guide to the Romagna Apennine geology. The Lamone valley, in: Fossil Vertebrates in the Lamone Valley, Romagna Apennines, Field Trip Guidebook, C. De Giuli and G.B. Vai, eds., pp. 7–37, 1989.

[35] G.B. Vai, Cyclostratigraphic estimate of the Messinian Stage duration, in: Miocene Integrated Stratigraphic Sequence, A. Montanari, G.S. Odin and R. Coccioni, eds., Elsevier, Amsterdam, in press.

[36] R. Gersonde, Palaeoekologische und biostratigraphische Auswertung von Diatomeenassoziationen aus dem Messinian des Caltanisetta-Beckens (Sizilien) und einiger Vergleichsprofile in Südwest-Spanien, Nordwest-Algerien und auf Kreta, Thesis, 393 pp., Univ. Kiel, Kiel, 1980.

[37] F. Gautier, G. Clauzon, J.-P. Suc, J. Cravatte and D. Violanti, Age and durée de la crise de salinité messinienne, C.R. Acad. Sci. Paris 318, 1103–1109, 1994.

[38] N.J. Shackleton, M.A. Hall and D. Pate, Pliocene stable isotope stratigraphy of ODP site 846, Proc. ODP Sci. Results 138, in press, 1995.

[39] D.A. Hodell, R.H. Benson, D.V. Kent, A. Boersma and K. Rakic-El Bied, Magnetostratigraphic, biostratigraphic, and stable isotope stratigraphy of an Upper Miocene drill core from the Salé Briqueterie (northwest Morocco): A high-resolution chronology for the Messinian stage, Paleoceanography 9, 835–855, 1994

[40] G.B. Dalrymple, G.A. Izett, L.W. Snee and J.D. Obradovich, $^{40}Ar/^{39}Ar$ age spectra and total-fusion ages of tektites from Cretaceous–Tertiary boundary sedimentary rocks in the Beloc Formation, Haïti, US Geol. Surv. Bull. 2065, 20 pp., 1993.

[41] H.M. Pedley and M. Grasso, Controls on faunal and sediment cyclicity within the Tripoli and Calcare di Base basins (Late Miocene) of central Sicily, Palaeogeogr. Palaeoclimatol. Palaeoecol. 105, 337–360, 1993.

[42] A. Decima, J.A. McKenzie and B.C. Schreiber, The origin of "evaporative" limestones: an example from the Messinian of Sicily (Italy), J. Sediment. Petrol. 58, 256–272, 1988.

[43] R.W.H. Butler, W.H. Lickorish, M. Grasso, H.M. Pedley and L. Ramberti, Tectonics and sequence stratigraphy in Messinian basins, Sicily: Constraints on the initiation and termination of the Mediterranean 'salinity crisis', Geol. Soc. Am. Bull. 107, 425–439, 1995.